

Journal of Materials Chemistry A

Accepted Manuscript



This is an *Accepted Manuscript*, which has been through the Royal Society of Chemistry peer review process and has been accepted for publication.

Accepted Manuscripts are published online shortly after acceptance, before technical editing, formatting and proof reading. Using this free service, authors can make their results available to the community, in citable form, before we publish the edited article. We will replace this *Accepted Manuscript* with the edited and formatted *Advance Article* as soon as it is available.

You can find more information about *Accepted Manuscripts* in the [Information for Authors](#).

Please note that technical editing may introduce minor changes to the text and/or graphics, which may alter content. The journal's standard [Terms & Conditions](#) and the [Ethical guidelines](#) still apply. In no event shall the Royal Society of Chemistry be held responsible for any errors or omissions in this *Accepted Manuscript* or any consequences arising from the use of any information it contains.



ARTICLE

Photocatalytic Hydrogen Generation on Bifunctional Ternary Heterostructured $\text{In}_2\text{S}_3/\text{MoS}_2/\text{CdS}$ Composite with High Activity and Stability under Visible Light Irradiation

Received 00th January 20xx,
Accepted 00th January 20xx

DOI: 10.1039/x0xx00000x

www.rsc.org/

Wenjun Jiang, Yanfang Liu, Ruilong Zong, Zhanping Li, Wenqing Yao and Yongfa Zhu*

Bifunctional ternary heterostructured $\text{In}_2\text{S}_3/\text{MoS}_2/\text{CdS}$ composite photocatalyst with high activity and stability under visible light irradiation was fabricated via a simple hydrothermal method. The bifunctional ternary heterostructured photocatalyst displayed higher activity for photocatalytic hydrogen evolution than GO/CdS and rGO/CdS composites and can be compared with the hydrogen-generating efficiency of systems containing the well-known Pt co-catalyst. But above all, the photocorrosion of CdS was also suppressed effectively. The heterojunction structure between MoS_2 and CdS promoted the interfacial charge transfer process, suppressed the charge recombination and enhanced the performance of photocatalytic hydrogen generation. Due to the well matching of the VB of CdS with that of In_2S_3 , holes on the VB of CdS could be easily transferred to that of In_2S_3 via the heterojunction structure between In_2S_3 and CdS, which prevented the accumulation of holes on the VB of CdS, inhibited its photocorrosion and dramatically enhanced its stability. The structure sequence and deposition site play an important role on photocatalytic activity: MoS_2 deposited on the interface of CdS and In_2S_3 was more efficient in promoting charge transfer and thus significantly improved the photocatalytic activity of the composite photocatalyst. Our findings pave a way to design bifunctional CdS-based ternary heterostructured composites for highly efficient H_2 generation and photocorrosion suppression.

Introduction

Photocatalytic hydrogen generation from water on photocatalysts with heterojunction has attracted increasing attention in the past four decades.¹⁻⁷ Among the photocatalysts, cadmium sulfide (CdS) is one of the most promising semiconductor materials. The bandgap of CdS is around 2.4 eV, which matches well with the visible range of solar irradiation. As a visible-light-driven photocatalyst with effective absorption of solar energy, it has been extensively investigated.⁸⁻¹² The construction of heterojunction is an effective way to improve photocatalytic activity thanks to the efficient interfacial charge transfer.^{3, 9, 10, 13, 14} Among various cocatalysts, MoS_2 is probably one of the most ideal candidates to enhance light harvesting and promote photogenerated charge separation via the interfaces. C. Li et al. reported that the activity of CdS can be enormously increased by depositing MoS_2 as a cocatalyst, and the activity of MoS_2/CdS could be even higher than that of Pt/CdS under the same reaction conditions.¹⁵ However, there is an inherent drawback for CdS-

based photocatalysts: the photocorrosion problem, in which the sulfide ion is highly prone to oxidation by photogenerated holes.^{16, 17} The photocorrosion effect makes CdS very unstable as a photocatalyst and greatly obstructs its practical application. It is therefore absolutely vital to develop suitable methods to inhibit photocorrosive damage to the CdS nanoparticles. Many researches were carried on to solve this problem. X.W. Lou et al. developed a method of coating CdS with a thin layer of amorphous carbon to stabilize the surface and inhibit the photocorrosion process.¹⁸ H. M. Cheng et al. fabricated CdS–mesoporous ZnS core–shell particles with high stability through a one-pot surfactant-free hydrothermal route.¹⁹ H. Q. Yu et al. fabricated an N-doped Graphene/CdS nanocomposite to enhance the stability of CdS.²⁰ H. X. Li developed a method of in situ sulfurization under supercritical conditions to stabilize CdS.²¹ Our group once developed a method of monolayer polyaniline hybridization to inhibit photocorrosion.²² These methods were a little bit complicated in some ways. Therefore, a more facile method of inhibiting photocorrosion is still required.

In this work, a simple hydrothermal method to fabricate bifunctional ternary heterostructured $\text{In}_2\text{S}_3/\text{MoS}_2/\text{CdS}$ composite with high activity and stability under visible light irradiation was established. Such an architecture provides a broadening optical window for effective light harvesting, short diffusion distance for excellent charge transport, as well as a large contact area for fast interfacial charge separation and photoelectrochemical reactions. The most interesting is that

Department of Chemistry, Tsinghua University, Beijing 100084, China.
E-mail: zhuyf@mail.tsinghua.edu.cn; Fax: +86-10-62787601; Tel: +86-10-62787601

† Footnotes relating to the title and/or authors should appear here.
Electronic Supplementary Information (ESI) available: [details of any supplementary information available should be included here]. See DOI: 10.1039/x0xx00000x

ARTICLE

Journal of Materials Chemistry A

the nanojunction is also anticipated to inhibit photocorrosive damage to the CdS nanorods. As a result, the ternary heterostructured $\text{In}_2\text{S}_3/\text{MoS}_2/\text{CdS}$ composite exhibits high stability.

Experimental Section

Synthesis

All the chemicals were purchased from SCRC, Shanghai. Deionized water was used throughout.

(a) *Preparation of the pure CdS nanorods.* 2 g Cadmium acetate dehydrate [$\text{Cd}(\text{Ac})_2 \cdot 2\text{H}_2\text{O}$] and 1 g thioacetamide (TAA) were added into 45 mL ethylenediamine [$\text{C}_2\text{H}_8\text{N}_2$] and stirred for 15 min until a dispersion was formed. Then it was transferred to a 100 mL Teflon-lined autoclave and heated at 200 °C for 3 h. After the reaction, the product was washed with deionized water through centrifugation for several times. The resulting yellow powder was dried in a vacuum oven at 80 °C.

(b) *Preparation of the pure MoS_2 .*²³ 42 mg Sodium molybdate dihydrate [$\text{Na}_2\text{MoO}_4 \cdot 2\text{H}_2\text{O}$] and 84 mg thiourea [$\text{CH}_4\text{N}_2\text{S}$] were added into 20 mL deionized water and stirred for 1 h. Then the resulting mixture was transferred to a 100 mL Teflon-lined autoclave and heated at 210 °C for 24 h. A dark gray precipitate resulted, which was centrifugated and then washed with deionized water before being dried in a vacuum oven at 80 °C.

(c) *Preparation of the pure In_2S_3 .*²⁴ An appropriate amount of $\text{InCl}_3 \cdot 4\text{H}_2\text{O}$ was dissolved in deionized water. The pH value of the solution was adjusted to 1.0 by adding hydrochloric acid to prevent the hydrolysis of $\text{InCl}_3 \cdot 4\text{H}_2\text{O}$. An appropriate amount of Na_2S solution was gradually added to the solution, with continuous stirring, to give a homogeneous yellow sol (the mol ratio of In:S=1:2.5). Then the pH value of this sol was adjusted to 3.0 by adding a dilute hydrochloric acid. Then the sol was transferred to a 100 mL Teflon-lined autoclave and heated at 160 °C for 24 h. An orange red precipitate resulted, which was centrifugated and then washed with deionized water before being dried in a vacuum oven at 80 °C.

(d) *Preparation of the MoS_2/CdS nanojunction.* 300 mg CdS, 0.907 mg $\text{Na}_2\text{MoO}_4 \cdot 2\text{H}_2\text{O}$ and 1.814 mg $\text{CH}_4\text{N}_2\text{S}$ was dispersed in 20 mL deionized water and stirred for 1 h. Then the resulting mixture was transferred to a 100 mL Teflon-lined autoclave and heated at 210 °C for 24 h. The precipitate was centrifugated and then washed with deionized water before being dried in a vacuum oven at 80 °C.

(e) *Preparation of the $\text{In}_2\text{S}_3/\text{CdS}$ nanojunction.* 300 mg CdS and 107.98 mg $\text{InCl}_3 \cdot 4\text{H}_2\text{O}$ was dissolved in 35 mL deionized water. The pH value of the solution was adjusted to 1.0 by adding hydrochloric acid to prevent the hydrolysis of $\text{InCl}_3 \cdot 4\text{H}_2\text{O}$. 220.96 mg $\text{Na}_2\text{S} \cdot 9\text{H}_2\text{O}$ was dissolved in 15 mL deionized water and was gradually added to the above solution, with continuous stirring, to give a homogeneous yellow sol (the mol ratio of In:S=1:2.5). Then the pH value of this sol was adjusted to 3.0 by adding a dilute hydrochloric acid. Then the sol was transferred to a 100 mL Teflon-lined autoclave and heated at

160 °C for 24 h. The precipitate resulted was centrifugated and then washed with deionized water before being dried in a vacuum oven at 80 °C.

(f) *Preparation of the $\text{In}_2\text{S}_3/\text{CdS}/\text{MoS}_2$ nanojunction.* 300 mg $\text{In}_2\text{S}_3/\text{CdS}$, 0.907 mg $\text{Na}_2\text{MoO}_4 \cdot 2\text{H}_2\text{O}$ and 1.814 mg $\text{CH}_4\text{N}_2\text{S}$ was dispersed in 20 mL deionized water and stirred for 1 h. Then the resulting mixture was transferred to a 100 mL Teflon-lined autoclave and heated at 210 °C for 24 h. The precipitate was centrifugated and then washed with deionized water before being dried in a vacuum oven at 80 °C.

(g) *Preparation of the $\text{In}_2\text{S}_3/\text{MoS}_2/\text{CdS}$ nanojunction.* 300 mg MoS_2/CdS and 107.98 mg $\text{InCl}_3 \cdot 4\text{H}_2\text{O}$ was dissolved in 35 mL deionized water. The pH value of the solution was adjusted to 1.0 by adding hydrochloric acid to prevent the hydrolysis of $\text{InCl}_3 \cdot 4\text{H}_2\text{O}$. 220.96 mg $\text{Na}_2\text{S} \cdot 9\text{H}_2\text{O}$ was dissolved in 15 mL deionized water and was gradually added to the above solution, with continuous stirring, to give a homogeneous yellow sol (the mol ratio of In:S=1:2.5). Then the pH value of this sol was adjusted to 3.0 by adding a dilute hydrochloric acid. Then the sol was transferred to a 100 mL Teflon-lined autoclave and heated at 160 °C for 24 h. The precipitate resulted was centrifugated and then washed with deionized water before being dried in a vacuum oven at 80 °C.

The working electrodes were prepared by dipping coating method: 10 mg of photocatalyst was suspended in 1ml DI water and then ultrasonic for 30 min to make a slurry, the slurry was then dip-coated onto a 2 cm×4 cm indium-tin oxide glass electrode. The electrodes were then exposed to UV light for 12 h to eliminate water and calcined at 100 °C for 1h.

Characterization

Morphologies of the prepared samples were examined with transmission electron microscopy (TEM) by a Hitachi HT 7700 electron microscope operated at an accelerating voltage of 100 kV. High resolution transmission electron microscopy (HRTEM) images were obtained by JEM 2100F field emission transmission electron microscope with an accelerating voltage of 200kV. FESEM images were captured on a Hitachi SU-8010 Field Emission Gun Scanning Electron Microscopy. X-ray photoelectron spectroscopy (XPS) was measured in a PHI 5300 ESCA system. The beam voltage was 3.0 kV, and the energy of Ar ion beam was 1.0 keV. The binding energies were normalized to the signal for adventitious carbon at 284.8 eV. The diffuse reflectance absorption spectra (DRS) of the samples were recorded in the range of 200-900nm on a UV-vis spectrophotometer (Hitachi UV-3010) equipped with an integrated sphere attachment, and BaSO_4 was used as a reference. X-ray diffraction (XRD) patterns of the powders were recorded at room temperature by a Bruker D8 Advance X-ray diffractometer at 40kV and 40mA for monochromatized $\text{Cu K}\alpha$ ($\lambda=1.5406 \text{ \AA}$) radiation. Raman spectra were recorded on a microscopic confocal Raman spectrometer (HORIBA HR800) with an excitation of 514.5 nm laser light. Fourier transform infrared (FT-IR) spectra were carried out using Bruker V70 spectrometer in the frequency of 3100-800 cm^{-1} with a resolution of 1 cm^{-1} . Electrochemical and photoelectrochemical measurements were performed in a

three-electrode quartz cells with 0.1 M Na₂SO₄ electrolyte solution. Platinum wire was used as counter electrode and saturated calomel electrode (SCE) used as reference electrode, respectively, and sample films electrodes on ITO served as the working electrode. The photoelectrochemical experiment results were recorded with an electrochemical system (CHI-660D, China).

Photocatalytic evaluation

The photocatalytic activities of the as-prepared samples were evaluated by the Perfect Light agitated reactor (LabSolar-III AG). Visible light source was obtained by a 300W Xe lamp with a 420 nm cut off filter. 50 mg photocatalyst was added into 100 mL solution (90 mL deionized water and 10 mL sacrificial agent). Before the light irradiation, the suspensions were firstly ultrasonic dispersed in dark for 30 min. At given time intervals (1 h), a certain amount of gas was taken from the reactor for gas concentration analysis using an online gas chromatograph (GC-7800) with a thermal conductivity detector (TCD) and using N₂ as carrier gas. Product gases were calibrated with standard H₂ gas and their identity were determined according to the retention time.

Results and Discussion

Structure and Morphology

The overall synthetic procedure of the ternary heterostructured In₂S₃/CdS/MoS₂ and In₂S₃/MoS₂/CdS composites is illustrated in Fig. 1 (see the Experimental Section for details). The difference in synthesizing these two composites is the sequence when MoS₂ is deposited on CdS. This different deposition sequence results in different microstructures, which are revealed by Transmission Electron Microscopy (TEM) and Field Emission Scanning Electron Microscopy (FESEM) images (shown in Fig. S1). As shown in Fig. 2a-2c, pure CdS, MoS₂ and In₂S₃ are nanorods, thin flakes and nanoparticles, respectively. Fig. 2d-2e shows the TEM images of the binary heterostructures. In MoS₂/CdS, a small amount of MoS₂ is coated on the surface of the CdS nanorods (insert of Fig. 2d), which forms the MoS₂/CdS heterostructures. In In₂S₃/CdS heterostructures, In₂S₃ is coated on the surface of the CdS nanorods (insert of Fig. 2e), forming the In₂S₃/CdS heterostructures. Fig. 2f-2g shows the TEM image of the ternary heterostructures. Both MoS₂ and In₂S₃ are coated on the surface of the CdS nanorods forming the ternary heterostructures. However, the deposition sites of MoS₂ between In₂S₃/CdS/MoS₂ and In₂S₃/MoS₂/CdS were quite different. For the former, MoS₂ was distributed on the surface of CdS (shown in the schematic plot of Fig. 2f). For the latter, MoS₂ was distributed on the interface of CdS and In₂S₃ (shown in the schematic plot of Fig. 2g), which is beneficial to charge transfer between CdS and In₂S₃ and gives full play to the charge transfer role of MoS₂. To test the idea still further, high resolution transmission electron microscopy (HRTEM) images of the In₂S₃/CdS/MoS₂ and In₂S₃/MoS₂/CdS heterostructures were observed. As can be seen in Fig. 2h-2i, the (002) plane of CdS, the (111) plane of In₂S₃ and the (002) plane of MoS₂

coexist in both the In₂S₃/CdS/MoS₂ and In₂S₃/MoS₂/CdS heterostructures. However, in In₂S₃/CdS/MoS₂ heterostructures, the MoS₂ was deposited on the surface of CdS, whereas in In₂S₃/MoS₂/CdS heterostructures, MoS₂ was deposited on the interface of CdS

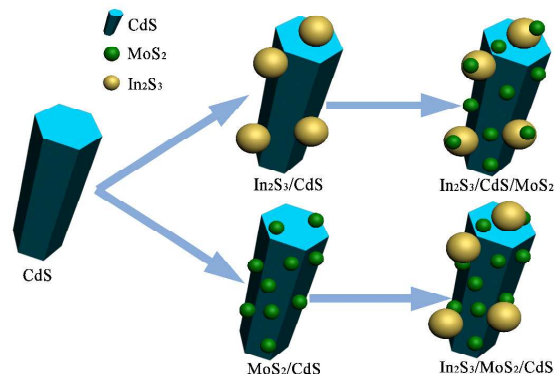


Fig. 1 Scheme of the preparation of heterostructured composites.

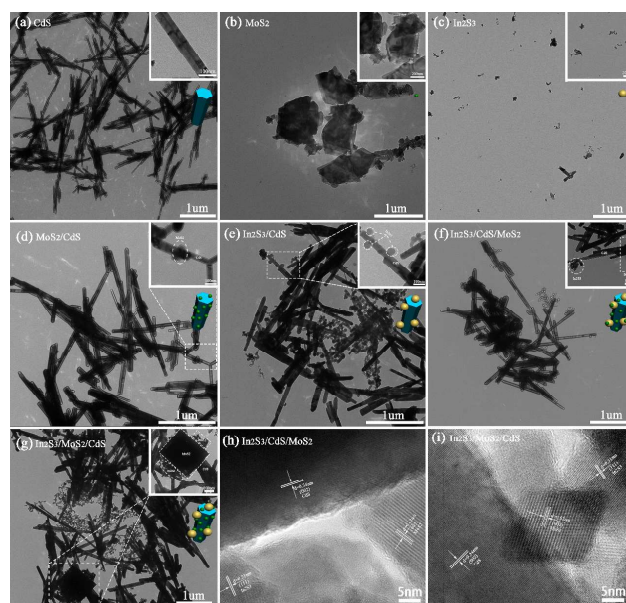


Fig. 2 TEM images of (a) pure CdS nanorods, (b) pure MoS₂, (c) pure In₂S₃, (d) MoS₂/CdS heterostructures (0.2 wt% of MoS₂), (e) In₂S₃/CdS heterostructures (20% wt% of In₂S₃), (f) In₂S₃/CdS/MoS₂ heterostructures (0.2 wt% of MoS₂ and 20 wt% of In₂S₃) and (g) In₂S₃/MoS₂/CdS heterostructures (0.2 wt% of MoS₂ and 20 wt% of In₂S₃). HRTEM images of (h) In₂S₃/CdS/MoS₂ heterostructures and (i) In₂S₃/MoS₂/CdS heterostructures.

and In₂S₃ and it is speculated that this unique structure was more in favor of charge transfer.

Fig. 3a shows the UV-vis DRS spectra of different samples. As expected, a sharp fundamental absorption edge rises at 520 nm for CdS. Since MoS₂ is in favour of light harvesting, the absorption intensity of MoS₂/CdS increased in the ultraviolet region compared with the pure CdS. Similarly, the absorption

intensity of $\text{In}_2\text{S}_3/\text{CdS}$ and $\text{In}_2\text{S}_3/\text{CdS}/\text{MoS}_2$ also increased drastically in the ultraviolet region compared with the pure CdS. As MoS_2 is black and is in favor of light harvesting, the more MoS_2 exposed to the surface of the samples, the stronger the absorption intensity is. The absorption intensity of $\text{In}_2\text{S}_3/\text{CdS}/\text{MoS}_2$ is stronger than that of $\text{In}_2\text{S}_3/\text{MoS}_2/\text{CdS}$, which

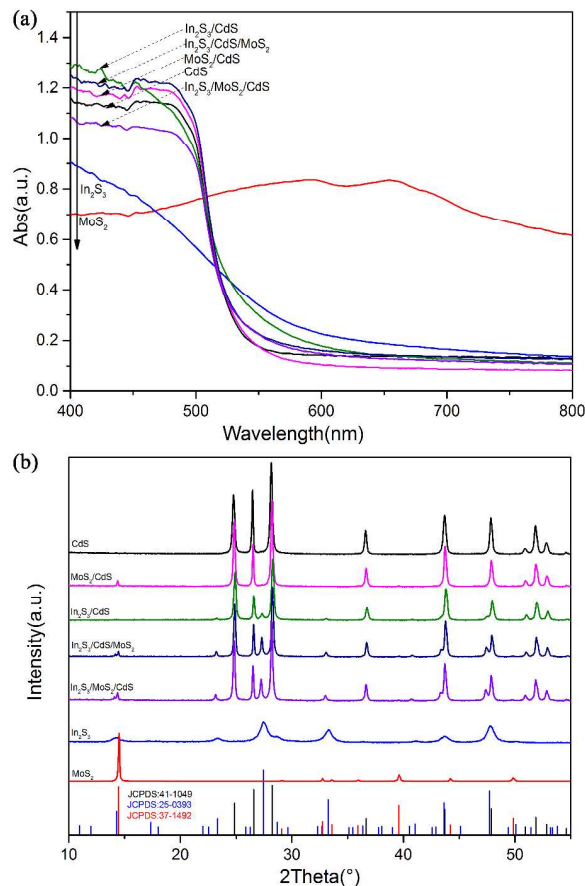


Fig. 3 (a) UV-vis absorption spectra and (b) XRD patterns of pure CdS nanorods, pure MoS_2 , pure In_2S_3 , MoS_2/CdS , $\text{In}_2\text{S}_3/\text{CdS}$, $\text{In}_2\text{S}_3/\text{CdS}/\text{MoS}_2$ and $\text{In}_2\text{S}_3/\text{MoS}_2/\text{CdS}$ heterostructures.

demonstrates that MoS_2 on $\text{In}_2\text{S}_3/\text{CdS}/\text{MoS}_2$ is exposed to the surface of CdS and In_2S_3 whereas MoS_2 on $\text{In}_2\text{S}_3/\text{MoS}_2/\text{CdS}$ is deposited on the interface of CdS and In_2S_3 .

Fig. 3b shows the XRD patterns of different samples. As shown in the Fig.3b, the diffraction peaks of CdS fit well with JCPDS:41-1049, indicating that CdS is hexagonal. The diffraction peaks of In_2S_3 fit well with JCPDS:25-0393, indicating that In_2S_3 is tetragonal. The diffraction peaks of MoS_2 fit well with JCPDS:37-1492, indicating that MoS_2 is hexagonal. Both the diffraction peaks of CdS and that of In_2S_3 were detected in $\text{In}_2\text{S}_3/\text{CdS}$, $\text{In}_2\text{S}_3/\text{CdS}/\text{MoS}_2$ and $\text{In}_2\text{S}_3/\text{MoS}_2/\text{CdS}$, which demonstrates that In_2S_3 was successfully deposited on CdS. Both the diffraction peaks of CdS and that of MoS_2 were detected in MoS_2/CdS ,

$\text{In}_2\text{S}_3/\text{CdS}/\text{MoS}_2$ and $\text{In}_2\text{S}_3/\text{MoS}_2/\text{CdS}$, which demonstrates that MoS_2 was successfully deposited on CdS.

XPS survey spectra (Fig. S2a) shows that the $\text{In}_2\text{S}_3/\text{MoS}_2/\text{CdS}$ heterostructures are mainly composed of S, In, Cd and Mo. The high-resolution XPS spectra of the C1s, S2p, Cd3d, In3d and Mo3d were shown in Fig. 4b-f. The high-resolution XPS spectra of C1s (Fig. S2b) was at 284.78 eV, corresponding to the carbonaceous pollution. As shown in Fig. S2c, the double peaks

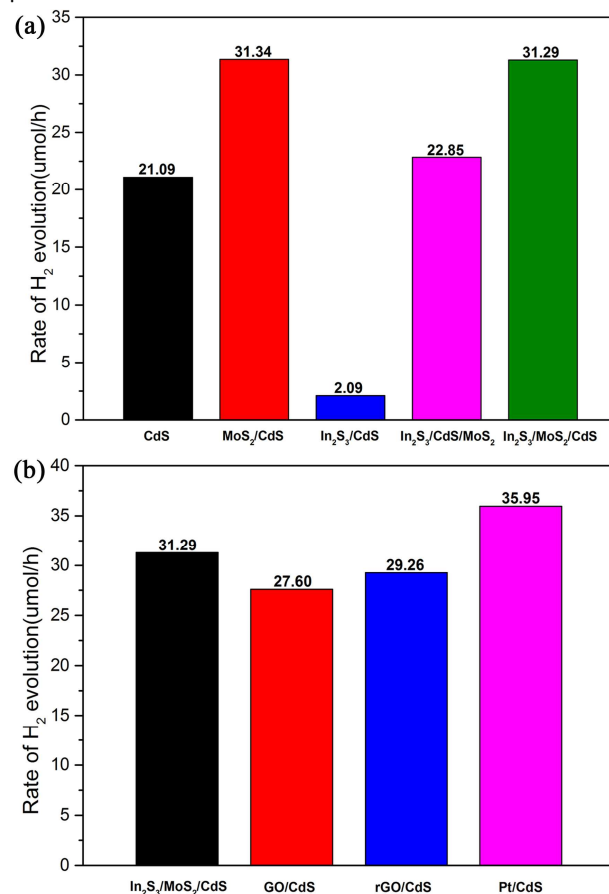


Fig. 4 (a) Rate of H_2 evolution on the pure CdS nanorods, MoS_2/CdS , $\text{In}_2\text{S}_3/\text{CdS}$, $\text{In}_2\text{S}_3/\text{CdS}/\text{MoS}_2$ and $\text{In}_2\text{S}_3/\text{MoS}_2/\text{CdS}$ heterostructures under visible light. (b) Rate of H_2 evolution on $\text{In}_2\text{S}_3/\text{MoS}_2/\text{CdS}$, GO/CdS, rGO/CdS and Pt/CdS. Reaction conditions: catalyst, 0.05 g; 100 ml solution containing 10 ml sacrificial reagent (lactic acid); light source (300W Xe Lamp) with a cutoff filter ($\lambda > 420$ nm).

for S2p were found at 162.62 eV and 161.93 eV, corresponding to the $\text{S}2\text{p}_{1/2}$ and $\text{S}2\text{p}_{3/2}$.¹⁶ As shown in Fig. S2d, the double peaks for Cd3d were found at 411.67 eV and 404.97 eV, corresponding to the $\text{Cd}3\text{d}_{3/2}$ and $\text{Cd}3\text{d}_{5/2}$.¹⁶ As shown in Fig. S2e, the double peaks for In3d were found at 451.99 eV and 444.39 eV, corresponding to the $\text{In}3\text{d}_{3/2}$ and $\text{In}3\text{d}_{5/2}$. As shown in Fig. S2f, the binding energies of Mo3d are 232.18 eV ($\text{Mo}3\text{d}_{3/2}$) and 229.08 eV ($\text{Mo}3\text{d}_{5/2}$). The above XPS data demonstrate that ternary heterostructured $\text{In}_2\text{S}_3/\text{MoS}_2/\text{CdS}$ composite was successfully fabricated.

Photocatalytic Properties and Mechanism

The rate of H₂ evolution on CdS using lactic acid, methanol and triethanolamine as the sacrificial reagents was shown in Fig. S3a. CdS alone exhibited extremely low activity for H₂ evolution without any sacrificial reagents. The rate of H₂ evolution on CdS with different sacrificial reagents is in the order of lactic acid > methanol > triethanolamine. Therefore, lactic acid was selected as the sacrificial reagent. Fig. S3b shows the rate of H₂ evolution on MoS₂/CdS binary heterostructured photocatalysts with

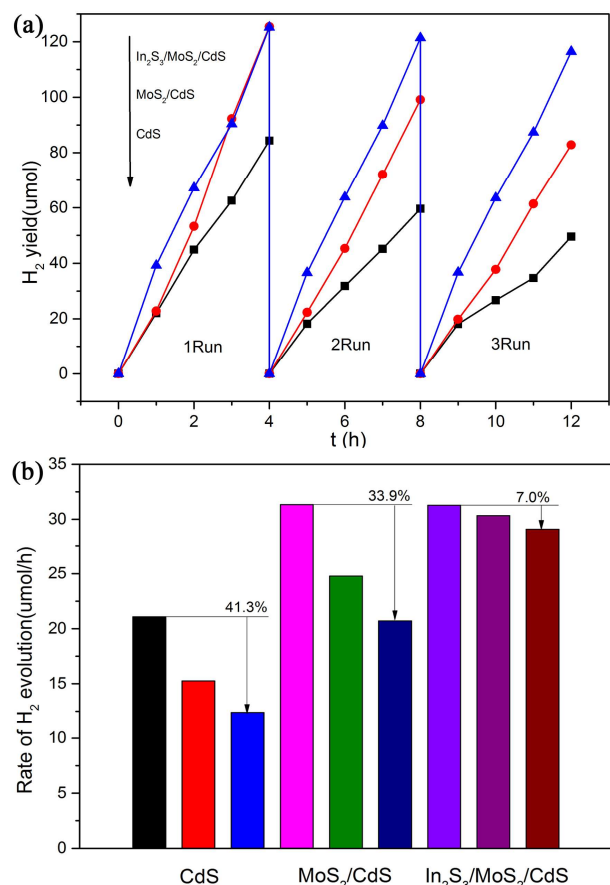


Fig. 5 (a) Time-circle H₂ evolution kinetics traces on the pure CdS nanorods, MoS₂/CdS and In₂S₃/MoS₂/CdS heterostructures. (b) Time-circle photocatalytic H₂ evolution rate on the pure CdS nanorods, MoS₂/CdS and In₂S₃/MoS₂/CdS heterostructures. Reaction conditions: catalyst, 0.05 g; 100 ml solution containing 10 ml sacrificial reagent (lactic acid); light source (300W Xe Lamp) with a cutoff filter ($\lambda > 420$ nm). No additional sacrificial reagents were added in the cycle test.

different MoS₂ contents. The sample of MoS₂/CdS-0.2% shows the highest photocatalytic activity.

Fig. 4a shows rate of H₂ evolution on the pure CdS nanorods, MoS₂/CdS, In₂S₃/CdS, In₂S₃/CdS/MoS₂ and In₂S₃/MoS₂/CdS heterostructures under visible light. Pure In₂S₃ and MoS₂ almost have no activity for hydrogen evolution. The rate of H₂ evolution on the pure CdS nanorods was about 21.09 μmol/h. In the first cycle test (Fig. 5a), the hydrogen production rate keeps constant with time going on, indicating that CdS was stable in the first four hours. However, after three cycles, the rate of H₂ evolution on CdS decreased by 41.3% (Fig. 5b),

indicating that the stability of CdS was quite poor. The nanorod structure of CdS was seriously damaged to irregular particles (shown in Fig. S4a2), which indicates that photocorrosion of CdS is quite serious. After depositing 0.2 wt% of MoS₂ as cocatalyst, the rate of H₂ evolution was increased by 48.6% (Fig. 4a), indicating that MoS₂ can promote the charge transfer on the interface and enhance the performance of photocatalytic hydrogen generation.¹⁶ Fig. S5I schematically illustrates the photocatalytic process of the nano hybrids. Upon photoexcitation, the electron-hole pairs can be generated in CdS nanorods. Owing to the nanojunction between CdS and MoS₂, the electrons can quickly diffuse to the surface of CdS nanorods and directly react with H⁺ in water to produce H₂. Meanwhile, the holes are mainly consumed by the lactic acid to generate CO₂. However, the photocorrosion of CdS is still serious, the nanorod structure of CdS was seriously damaged to irregular particles (shown in Fig. S4b2) and the rate of H₂ evolution of MoS₂/CdS decreased by 33.9% after three cycles (shown in Fig. 5b). After depositing In₂S₃ to CdS nanorods, the rate of H₂ evolution on In₂S₃/CdS decreased substantially (Fig. 4a), which demonstrates that the deposition of In₂S₃ lowers photocatalytic activity. However, the photocorrosion of CdS was inhibited. After three cycles, the nanorod structure of CdS still kept intact (Fig. S4c2). The probable reasons are as follows (Fig. S5II): due to the well matching of the VB of CdS with that of In₂S₃,^{24, 25} electrons on the CB of In₂S₃ could be easily transferred to that of CdS and holes on the VB of CdS could be easily transferred to that of In₂S₃ via the heterojunction structure between In₂S₃ and CdS under visible light irradiation. The photocatalytic oxidation reaction occurred on the VB of In₂S₃, which prevented the accumulation of holes on the VB of CdS, inhibited corrosion inhibition of CdS and enhanced the stability of photocatalyst. However, the oxidation of water is the rate determining step for photocatalytic hydrogen generation. The oxidizing capacity of holes decreased after being transferred to VB of In₂S₃ from that of CdS and the reduced capacity of electrons also decreased after being transferred to CB of CdS from that of In₂S₃, which leads to the decrease of hydrogen production performance.

For the sake of both inhibiting photocorrosion and promoting hydrogen generation performance, the bifunctional ternary heterostructured In₂S₃/MoS₂/CdS composite was fabricated. Interestingly, In₂S₃/CdS/MoS₂ and In₂S₃/MoS₂/CdS showed different hydrogen generation performance, which indicates that structure sequence and deposition site have a great influence on photocatalytic activity. As shown in Fig. 4a, the photocatalytic activity of In₂S₃/CdS/MoS₂ increased by only 8.3% compared with that of CdS after depositing MoS₂ onto In₂S₃/CdS. However, the photocatalytic activity of In₂S₃/MoS₂/CdS increased by 48.4% compared with that of CdS after depositing In₂S₃ onto MoS₂/CdS, which is comparable to the photocatalytic activity of MoS₂/CdS. Fig. 4b shows rate of H₂ evolution on In₂S₃/MoS₂/CdS, GO/CdS, rGO/CdS and Pt/CdS. The bifunctional ternary heterostructured photocatalyst displayed higher activity for photocatalytic hydrogen evolution than GO/CdS and rGO/CdS composites and can be compared

with the hydrogen-generating efficiency of systems containing the well-known Pt co-catalyst.²⁶⁻²⁸ The cycle experiments (Fig. 5b) shows that the photocatalytic activity of $\text{In}_2\text{S}_3/\text{MoS}_2/\text{CdS}$ decreased by only 7.0% after three cycles, indicating that the photocatalytic stability of $\text{In}_2\text{S}_3/\text{MoS}_2/\text{CdS}$ is much better than that of pure CdS. The TEM image of $\text{In}_2\text{S}_3/\text{MoS}_2/\text{CdS}$ (Fig. S4e2) shows that the nanorod structure of CdS kept undamaged after three cycles, which indicates that the photocorrosion of CdS was inhibited effectively.

To investigate their photoelectrochemical properties, a three-electrode electrochemical setup was used to measure the

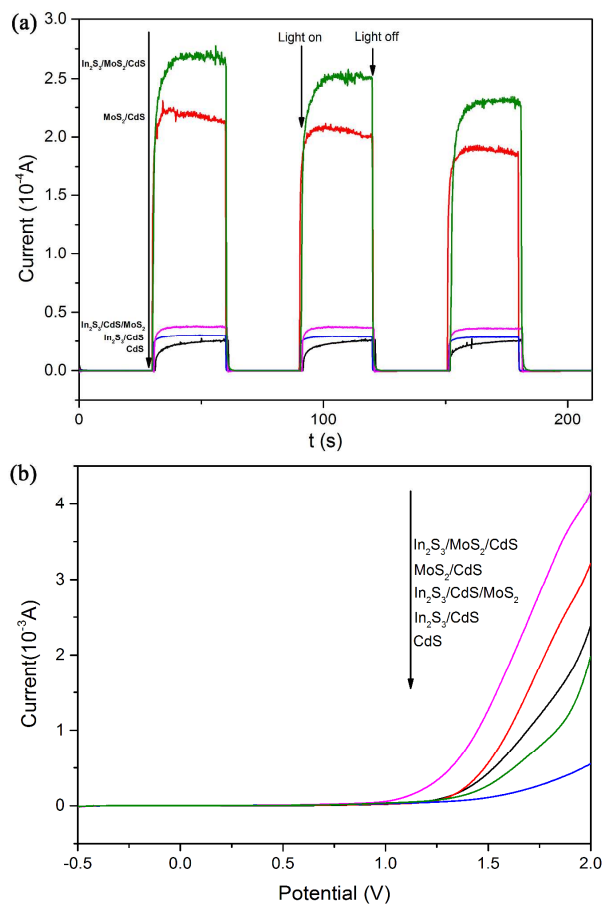


Fig. 6 (a) Transient photocurrent responses of the pure CdS nanorods, MoS_2/CdS , $\text{In}_2\text{S}_3/\text{CdS}$, $\text{In}_2\text{S}_3/\text{CdS}/\text{MoS}_2$ and $\text{In}_2\text{S}_3/\text{MoS}_2/\text{CdS}$ heterostructures. (b) Photocurrent-potential curves of the pure CdS nanorods, MoS_2/CdS , $\text{In}_2\text{S}_3/\text{CdS}$, $\text{In}_2\text{S}_3/\text{CdS}/\text{MoS}_2$ and $\text{In}_2\text{S}_3/\text{MoS}_2/\text{CdS}$ heterostructures.

photocurrent response. Fig. 6a shows the transient photocurrent responses of different samples. The transient photocurrent response of CdS was the minimum. The transient photocurrent response increased by 62% after depositing MoS_2 to CdS, indicating that MoS_2 can accelerate the charge transport¹⁶. The transient photocurrent response was 8 times as high as that of CdS after depositing In_2S_3 to CdS, indicating that the heterojunction between In_2S_3 and CdS can accelerate the charge separation²⁹. The transient photocurrent responses

of $\text{In}_2\text{S}_3/\text{CdS}/\text{MoS}_2$ and $\text{In}_2\text{S}_3/\text{MoS}_2/\text{CdS}$ were quite different, which implies that structure sequence and deposition site have great influence on charge migration and photocatalytic activity. For $\text{In}_2\text{S}_3/\text{CdS}/\text{MoS}_2$ (Fig. 7I), MoS_2 was distributed on the surface of CdS and In_2S_3 and almost no MoS_2 was distributed on the interface of CdS and In_2S_3 , which implies that MoS_2 accelerates the charge transfer only on the surface of CdS and In_2S_3 . Therefore the transient photocurrent response increased by only 28%. In contrast, for $\text{In}_2\text{S}_3/\text{MoS}_2/\text{CdS}$ (Fig. 7II), MoS_2 was distributed on the surface of CdS and in the interface of In_2S_3 and CdS, which implies that MoS_2 accelerates the charge transfer both on the surface of CdS and in the interface of In_2S_3

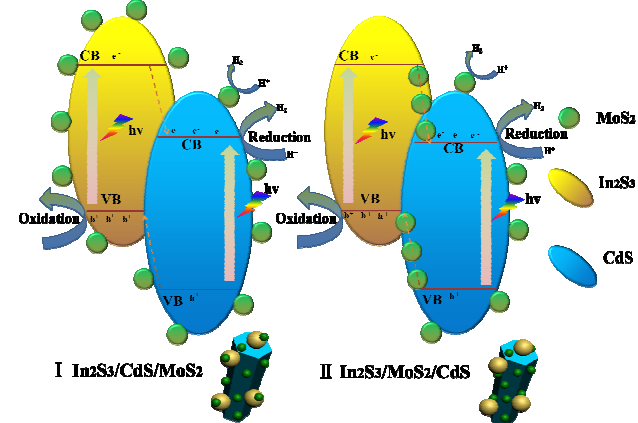


Fig. 7 Schematic illustration of the charge transfer and separation on the $\text{In}_2\text{S}_3/\text{CdS}/\text{MoS}_2$ and $\text{In}_2\text{S}_3/\text{MoS}_2/\text{CdS}$ heterostructures under visible light.

and CdS. Therefore, the transient photocurrent response was 10 times as high as that of CdS. Fig. 6b shows the photocurrent-potential curves of different samples. Almost no current response occurred until the bias potential at 1.0 eV, where the current obviously increased. With the increase of bias potential, the recombination of photoinduced electrons and holes was hindered, and the transfer of electrons to the external circuit can also be accelerated.³⁰ The photocurrent intensity of different samples at the same bias potential fit well with transient photocurrent responses (shown in Fig. 6a).

On the basis of the above analysis, a probable mechanism for different hydrogen generation performance are illustrated in Fig. 7. When depositing MoS_2 onto $\text{In}_2\text{S}_3/\text{CdS}$ (Fig. 7I), MoS_2 was distributed on the surface of CdS and In_2S_3 and almost no MoS_2 was distributed in the interface of CdS and In_2S_3 , which implies that MoS_2 accelerates the charge transfer only on the surface of CdS and In_2S_3 . In contrast, when depositing In_2S_3 to MoS_2/CdS (Fig. 7II), MoS_2 was distributed on the surface of CdS and in the interface of In_2S_3 and CdS, which implies that MoS_2 accelerates the charge transfer both on the surface of CdS and on the interface of In_2S_3 and CdS, and thus significantly improved the photocatalytic activity of the heterojunctions.

Conclusions

In conclusion, bifunctional ternary heterostructured $\text{In}_2\text{S}_3/\text{MoS}_2/\text{CdS}$ composite was fabricated via a simple hydrothermal method. The bifunctional ternary heterostructured $\text{In}_2\text{S}_3/\text{MoS}_2/\text{CdS}$ composite exhibits high activity and stability under visible light irradiation. The heterojunction structure between MoS_2 and CdS promoted the charge transfer on the interface, inhibited the recombination of electrons and holes and enhanced the performance of photocatalytic hydrogen generation. Holes in the VB of CdS could be easily transferred to that of In_2S_3 via the heterojunction structure between In_2S_3 and CdS under visible light irradiation, which prevented the accumulation of holes in the VB of CdS , inhibited corrosion inhibition of CdS and enhanced the stability of photocatalyst. The influence of structure sequence and deposition site on photocatalytic activity were also discussed: MoS_2 deposited on the interface of CdS and In_2S_3 was more in favor of charge transfer. This work paves a good way to design bifunctional CdS -based ternary heterostructured composites for highly efficient H_2 generation and photocorrosion suppression.

Acknowledgements

This work was partly supported by National Basic Research Program of China (973 Program) (2013CB632403), National High Technology Research and Development Program of China (863 Program) (2012AA062701) and Chinese National Science Foundation (21437003 and 21373121).

References

- 1 Y. Xu, Z. Lin, X. Huang, Y. Liu, Y. Huang and X. Duan, *ACS nano*, 2013, **7**, 4042-4049.
- 2 Y. Wang, R. Shi, J. Lin and Y. Zhu, *Energy & Environmental Science*, 2011, **4**, 2922-2929.
- 3 Z. Zhang, J. Huang, M. Zhang, Q. Yuan and B. Dong, *Applied Catalysis B: Environmental*, 2015, **163**, 298-305.
- 4 X. Xu, L. Hu, N. Gao, S. Liu, S. Wageh, A. A. Al-Ghamdi, A. Alshahrie and X. Fang, *Adv Funct Mater*, 2015, **25**, 445-454.
- 5 J. Zhao, T. Minegishi, L. Zhang, M. Zhong, Gunawan, M. Nakabayashi, G. Ma, T. Hisatomi, M. Katayama, S. Ikeda, N. Shibata, T. Yamada and K. Domen, *Angew Chem Int Edit*, 2014, **53**, 11808-11812.
- 6 H. N. Kim, T. W. Kim, I. Y. Kim and S.-J. Hwang, *Adv Funct Mater*, 2011, **21**, 3111-3118.
- 7 P. Rodenas, T. Song, P. Sudhagar, G. Marzari, H. Han, L. Badia-Bou, S. Gimenez, F. Fabregat-Santiago, I. Mora-Sero, J. Bisquert, U. Paik and Y. S. Kang, *Adv Energy Mater*, 2013, **3**, 176-182.
- 8 K. Wu, Z. Chen, H. Lv, H. Zhu, C. L. Hill and T. Lian, *Journal of the American Chemical Society*, 2014, **136**, 7708-7716.
- 9 Z. Zhang, C. Shao, X. Li, Y. Sun, M. Zhang, J. Mu, P. Zhang, Z. Guo and Y. Liu, *Nanoscale*, 2013, **5**, 606-618.
- 10 Z. Zhang, B. Dong, M. Zhang, J. Huang, F. Lin and C. Shao, *International Journal of Hydrogen Energy*, 2014, **39**, 19434-19443.
- 11 S. Han, L. Hu, N. Gao, A. A. Al-Ghamdi and X. Fang, *Adv Funct Mater*, 2014, **24**, 3725-3733.
- 12 C. Han, Z. Chen, N. Zhang, J. C. Colmenares and Y.-J. Xu, *Adv Funct Mater*, 2015, **25**, 221-229.
- 13 Z. Zhang, A. Li, S.-W. Cao, M. Bosman, S. Li and C. Xue, *Nanoscale*, 2014, **6**, 5217-5222.
- 14 Z. Zhang, Z. Wang, S.-W. Cao and C. Xue, *The Journal of Physical Chemistry C*, 2013, **117**, 25939-25947.
- 15 M. A. Montgomery and M. Elimelech, *Environmental Science & Technology*, 2007, **41**, 17-24.
- 16 J. Chen, X.-J. Wu, L. Yin, B. Li, X. Hong, Z. Fan, B. Chen, C. Xue and H. Zhang, *Angewandte Chemie*, 2015, **127**, 1226-1230.
- 17 R. Marschall, *Adv Funct Mater*, 2014, **24**, 2421-2440.
- 18 Y. Li, J. Rodrigues and H. Tomas, *Chemical Society Reviews*, 2012, **41**, 2193-2221.
- 19 Y. P. Xie, Z. B. Yu, G. Liu, X. L. Ma and H.-M. Cheng, *Energy Environ Sci*, 2014, **7**, 1895-1901.
- 20 G. Wang, Q. Chang, X. Han and M. Zhang, *Journal of Hazardous Materials*, 2013, **248-249**, 115-121.
- 21 Q. Chen, L. Zhu, C. Zhao, Q. Wang and J. Zheng, *Advanced Materials*, 2013, **25**, 4171-4176.
- 22 J. Xu, L. Wang and Y. Zhu, *Langmuir*, 2012, **28**, 8418-8425.
- 23 Y. Hou, Z. Wen, S. Cui, X. Guo and J. Chen, *Adv Mater*, 2013, **25**, 6291-6297.
- 24 Y. He, D. Li, G. Xiao, W. Chen, Y. Chen, M. Sun, H. Huang and X. Fu, *J Phys Chem C*, 2009, **113**, 5254-5262.
- 25 C. Eley, T. Li, F. Liao, S. M. Fairclough, J. M. Smith, G. Smith and S. C. E. Tsang, *Angew Chem Int Edit*, 2014, **53**, 7838-7842.
- 26 X.-J. Lv, W.-F. Fu, H.-X. Chang, H. Zhang, J.-S. Cheng, G.-J. Zhang, Y. Song, C.-Y. Hu and J.-H. Li, *Journal of Materials Chemistry*, 2012, **22**, 1539-1546.
- 27 P. Gao, J. Liu, S. Lee, T. Zhang and D. D. Sun, *Journal of Materials Chemistry*, 2012, **22**, 2292-2298.
- 28 Y. Wang, Y. Wang and R. Xu, *The Journal of Physical Chemistry C*, 2013, **117**, 783-790.
- 29 F. Yamaga, K. Washio and M. Morikawa, *Environmental science & technology*, 2010, **44**, 6470-6474.
- 30 J. Wang and W.-D. Zhang, *Electrochim Acta*, 2012, **71**, 10-16.